

## Polarization-Controlled Confined Tamm Plasmon Lasers

Guillaume Lheureux,<sup>†</sup> Stefano Azzini,<sup>†</sup> Clementine Symonds,<sup>\*,†</sup> Pascale Senellart,<sup>‡</sup> Aristide Lemaître,<sup>‡</sup> Christophe Sauvan,<sup>§</sup> Jean-Paul Hugonin,<sup>§</sup> Jean-Jacques Greffet,<sup>§</sup> and Joel Bellessa<sup>†</sup>

<sup>†</sup>Institut Lumière Matière, Université de Lyon, UMR5306 Université Claude Bernard Lyon1-CNRS, 69622 Villeurbanne, France

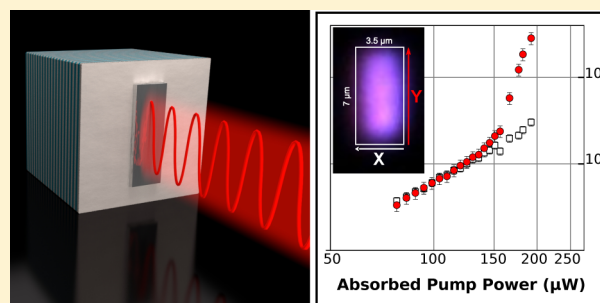
<sup>‡</sup>Laboratoire de Photonique et des Nanostructures, CNRS UPR20, Route de Nozay, F-91460 Marcoussis, France

<sup>§</sup>Laboratoire Charles Fabry, Institut d'Optique CNRS, Université Paris-Sud, 2 avenue Fresnel, 91127 Palaiseau, France

### S Supporting Information

**ABSTRACT:** In this paper we report on the evidence of polarized and spatially localized emission of a Tamm laser. The polarized emission results from an anisotropic three-dimensional confinement of Tamm plasmon modes at the interface between an active semiconductor distributed Bragg reflector and a silver thin-film. The spatial confinement is achieved by patterning microrectangles with an aspect ratio of 2 in the top metallic layer. This geometrical birefringence is observed to split the fundamental confined Tamm mode into two modes, which result to be orthogonally polarized along the two sides of the structure. We measure a wavelength splitting between the nondegenerate modes of  $\sim 0.2$  nm, which turns out to be in good agreement with numerical calculations. This weak splitting, together with the strong wavelength dependence of the buried quantum wells gain curve, allows us to demonstrate the existence of a highly linearly polarized laser emission at  $\sim 850$  nm. By controlling the detuning between the confined Tamm modes and the gain curve, we report on a maximum degree of linear polarization in excess of 90%.

**KEYWORDS:** Tamm plasmons, semiconductor lasers, polarization-controlled lasers, hybrid metal/dielectric structures, surface plasmons



The polarization of an electromagnetic field represents a crucial property for electromagnetic waves all over the spectrum. At optical wavelengths, the control of a well-defined polarization state of light is essential to various domains in photonics, ranging from spectroscopy to nonlinear optics, as well as optical communications and quantum information processing.<sup>1,2</sup> Polarized coherent light sources, that could eventually be integrated onto a semiconductor platform to meet miniaturization requirements, are always strongly needed.<sup>3</sup> In addition, important advances have been recently reported in the realization of integrated devices dealing with polarization-encoded photonic qubits, both at the source<sup>4</sup> and logical operation level.<sup>5</sup> Concerning polarized laser sources, different types of semiconductor lasers have been investigated over the years, that can feature single mode operation with high spectral purity, the most important constraints for applications.<sup>6</sup> Among them, vertical-cavity surface-emitting lasers (VCSELs) have been intensively studied in the last 20 years,<sup>7</sup> due to their practical advantages, such as compactness, circular beam shape, and easy array integration, that finally contribute to lowering production costs. However, the control of polarization remains an open problem for the use of VCSELs in polarization-sensitive applications, which makes them still subject of continuous research efforts.<sup>8–11</sup> Indeed, the linear TE polarization of a VCSEL is essentially randomly oriented in the plane of the semiconductor material quantum wells. As a result, they

suffer from current- and temperature-dependent polarization instabilities responsible for polarization switching of the single transverse lasing mode between two orthogonal linearly polarized states.<sup>12–14</sup> Many approaches have been proposed to solve this issue, mainly based on anisotropic gain mechanisms<sup>15,16</sup> or anisotropic transverse cavity geometries.<sup>17–20</sup> In particular, the latter approach has been proven to be a valuable technique for increasing the energy splitting between the two nearly degenerate polarizations,<sup>20</sup> thereby selecting a single specific polarization direction.<sup>18</sup> The best approaches trying to obtain a stable single-polarization regime are those who enhance the lasing operation in the fundamental mode. In this direction, the use of a defect state in a photonic band gap, namely, a defect in a photonic crystal (PhC) periodic structure, represents a promising approach. A considerable amount of experimental work has already been carried out on the fabrication of VCSELs incorporating a PhC structure in the top mirror:<sup>21–23</sup> results show the achievement of high output power ( $\sim$ milliWatt) single fundamental mode emission at a stable polarization, but at the expense of an accurate PhC design followed by a complex and involved fabrication procedure.

Recently, a novel type of hybrid metal–semiconductor photonic structure based on Tamm plasmon (TP) modes has

Received: December 15, 2014

Published: June 5, 2015

been proposed to control the spontaneous emission of a buried quantum emitter,<sup>24</sup> and it has already been demonstrated to allow for the realization of novel surface-wave lasers<sup>25</sup> and single photon<sup>26</sup> sources. TPs are electromagnetic defect states that can be formed at the interface of a thin-film metallic layer and a distributed Bragg reflector (DBR): their energy features an in-plane wave vector parabolic dispersion relation lying inside the DBR stop-band and within the light cone,<sup>27,28</sup> so that these modes can be optically directly accessed at normal incidence. Moreover, the Tamm resonance electric field is confined at the metal-DBR interface, and, since the field penetration inside the DBR is about 2 orders of magnitude larger than that in the metal layer, they present reduced losses compared to surface plasmons. Since their introduction in 2007 by Kaliteevski et al., TPs have already been theoretically proposed for the realization of perfect absorbers,<sup>29</sup> multichannel filters,<sup>30</sup> and bistable switches.<sup>31,32</sup> Furthermore, a few experimental results have been recently published in the literature, showing the large growing interest in Tamm structures, attractive because of their advantages with respect to surface plasmons. TPs have been proposed and demonstrated as a novel straightforward and promising tool to engineer fluorophores emission in terms of directionality, wavelength and decay rates.<sup>33–35</sup> TPs combined with mesoporous DBR have been proven to be successfully employed as high-sensitivity sensors in alternative to surface plasmons.<sup>36</sup> In addition, the coexistence of Tamm plasmon and surface plasmon modes in these hybrid metal/dielectric structures<sup>37,38</sup> could make of Tamm plasmon lasers a new approach for the development of novel efficient surface plasmon sources.

The peculiarity of TP lasers lies in the absence of a cavity layer, having the TP mode itself the role of the resonant cavity, which results in a compact device whose emission properties can thus be easily controlled directly by tailoring the optical mode. Generally, for a semiconductor-integrated laser source, important interventions are needed on the laser cavity in order to modify emission properties such as the far-field emission or directionality, the quality factor and the  $\beta$ -factor. TP lasers allow for a simplified control of such properties: instead of modifying an optical cavity which does not physically exist, it is sufficient to act on the metal geometry to directly shape the lasing mode itself. Indeed, it has been successfully demonstrated that three-dimensionally confined Tamm plasmons (CTPs) can be obtained only by patterning the top metallic layer,<sup>24</sup> without any degradation of the quantum wells (QWs) buried in the active part of the DBR. In particular, circular metallic geometries in the form of microdisks have been successfully employed for the demonstration of lasing action from a CTP mode, and a reduction of the lasing threshold with respect to bidimensional TPs has been reported.<sup>39</sup> However, these novel laser sources suffer from the same polarization issues mentioned above for VCSELs, as they are still surface emitting devices.

The use of asymmetry in the form of anisotropic cross sections, for example, elliptical or rectangular, represents a valuable solution in order to control a given polarization state of light in a device confining and guiding light.<sup>40</sup> Indeed, such a geometrical asymmetry is responsible to lift-off the energy degeneracy between the two orthogonal linear polarization modes oscillating along the two Cartesian direction of the plane. The introduction of strong geometrical birefringence has already been used for years in polarization maintaining optical fibers, and it also allowed to address polarization issues in both VCSELs<sup>13</sup> and semiconductor pillar microcavities.<sup>20</sup> Nevertheless, the fabrication of such devices comes at the cost of a

long and delicate technological process, comprising, among others, multiples lithography and etching steps, the latter possibly involving the active material as well. On the contrary, TP structures are based on an electromagnetic mode existing only at the metal-DBR interface. This offers the great advantage and capability of manipulating and confining the mode itself directly by patterning bidimensional geometries in the metallic layer, without affecting the semiconductor material. In this paper, exploiting the mode-tailoring capabilities offered by CTP structures, we propose to employ some geometrical birefringence to fix the polarization state of CTP lasers. Indeed, here we report on the first experimental study of anisotropic CTP (a-CTP) lasing devices. The use of anisotropic 2D metal geometries, that is, microrectangles, has been observed to increase enough the polarization splitting between the two confined degenerate fundamental modes as to produce a linearly polarized laser emission. The relevance of the energy detuning between the Tamm modes and the gain material has also been investigated, resulting to be the control mechanism for the emission of a single linearly polarized lasing mode.

## RESULTS AND DISCUSSION

**Sample Structure and Linear Characterization.** A typical a-CTP structure is presented in Figure 1a. It is composed by an active distributed Bragg reflector (DBR) formed by

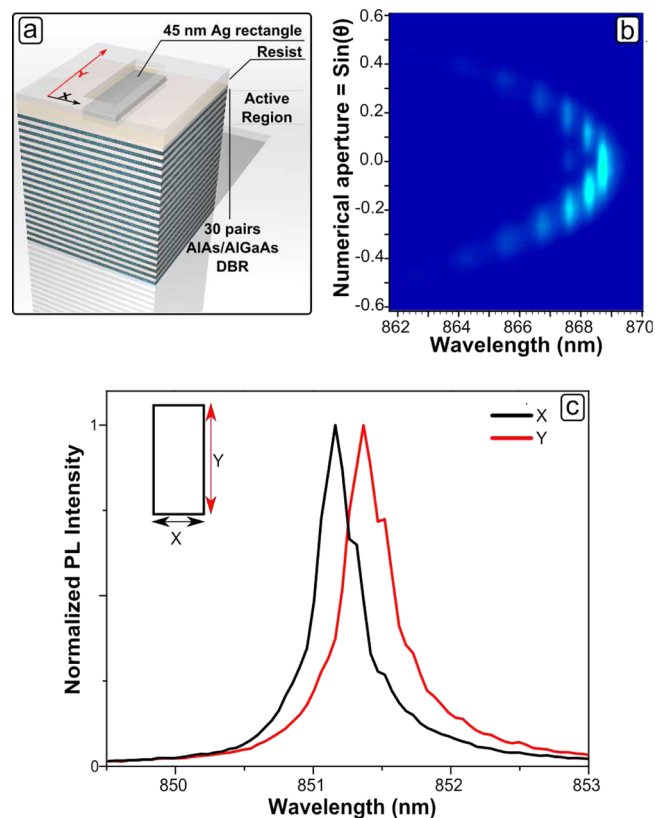


**Figure 1.** Anisotropic confined Tamm plasmons. (a) Schematic view of an anisotropic confined Tamm plasmon (a-CTP) laser device. The Tamm mode lies only beneath the metallic rectangle. (b) Unpolarized angle-resolved PL image taken on a  $6 \mu\text{m} \times 3 \mu\text{m}$  rectangle: Tamm plasmon resonances are largely detuned with respect to QW emission to ensure a weak coupling regime. (c) Polarization resolved PL emission spectra from a  $6 \mu\text{m} \times 3 \mu\text{m}$  device for two cross-polarizations: The X-polarized (black curve) and Y-polarized (red curve) a-CTP fundamental modes of a polarized laser device.

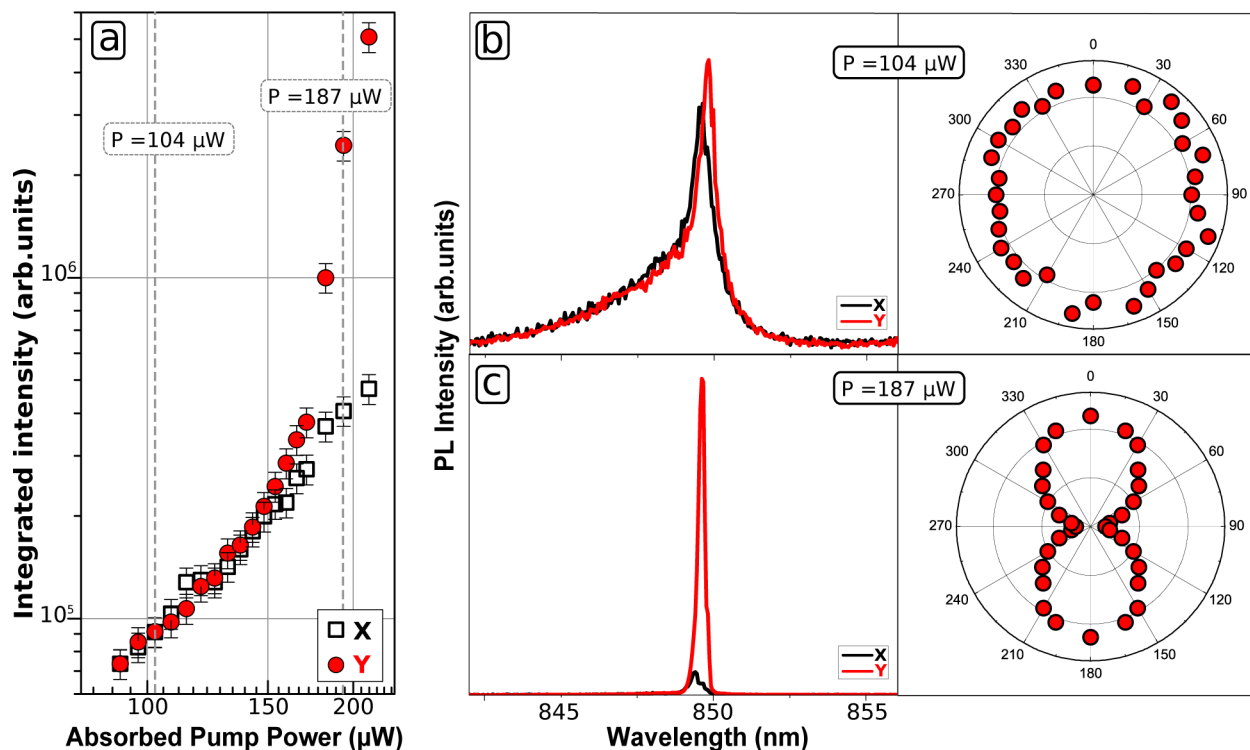


**Figure 2.** Experimental results from PL measurements on a  $7 \mu\text{m} \times 3.5 \mu\text{m}$  a-CTP device. (a) Integrated intensities of the X- and Y-polarized fundamental Tamm modes as a function of absorbed pump power  $P$ . (b, c) PL spectra and polar plot at  $P \sim 104 \mu\text{W}$  (below laser threshold) and  $P \sim 187 \mu\text{W}$  (above laser threshold), respectively. For representation convenience, the polar plot in (c) is obtained by symmetrization of experimental data in between  $0^\circ$  and  $180^\circ$ .

a 30 pairs AlAs/AlGaAs  $\lambda/4$  stacked layer grown on GaAs substrate by molecular beam epitaxy. Two 9.5 nm InGaAs semiconductor QWs, playing the role of active medium, are embedded in the five high-index upper layers, with optical emission lying around 856 nm at 77 K. In order to realize metallic patterns, a 90 nm thick PMMA resist layer was spin-coated on the top of the sample and several rectangular structures having aspect ratio of 2 were defined using electron beam lithography techniques. Finally, a 45 nm thick silver film was thermally evaporated on top of the DBR to allow for the formation of a TP mode only in the DBR region beneath the metallic layer. The chosen silver thickness represents a trade-off which allows to achieve a good quality factor while maintaining a sufficiently high extraction of the laser light. No lift-off was performed, as to mask QW emission from outside the Tamm structures.

The sample was kept at 77 K in a coldfinger cryostat and photoluminescence (PL) experiments were performed to study its optical properties. The devices were optically pumped from the top by means of a 80 MHz repetition-rate train of lasers pulses at 780 nm coming from a Ti:sapphire laser, focused onto the sample to a  $\sim 8 \mu\text{m}$  spot-size by a high-numerical aperture microscope objective (NA = 0.75), preceded by a two-lenses optical telescope controlling the beam size. The emitted light was collected using the same objective and sent to a monochromator coupled to a silicon CCD array. Angular resolved PL spectroscopy was performed using a Fourier lens imaging the back focal plane of the objective onto the entrance slits of the spectrometer (spectral resolution 0.1 nm, angular resolution  $0.3^\circ$ ). Along the same optical path, a rotating half-wave plate together with a polarizer cube were placed, to be able to measure any linear polarization state lying in the plane of the

sample. Figure 1b shows the PL intensity of a  $6 \mu\text{m} \times 3 \mu\text{m}$  rectangle as a function of wavelength and NA, measured at continuous-wave (CW) low-power excitation. The image was taken on a device characterized by a TP mode emission largely detuned at longer wavelengths with respect to QW emission: the photoemitted light is spontaneous emission from the exponential tail of the excitonic transition which comes to be enhanced by the TP modes themselves.<sup>41,42</sup> Such a detuning allows us to observe TP resonances avoiding any TP/exciton strong coupling<sup>43</sup> or lasing phenomena<sup>25</sup> to occur. The dispersion relation consists of a parabolic series of discrete resonance wavelengths, proving that the TP mode of an anisotropic Tamm device is actually confined in all three space dimensions, in a similar way as it was already observed for isotropic structures.<sup>24</sup> The vertical confinement comes from the very nature of a TP mode, while its lateral confinement is provided by the finite lateral dimensions of the metallic film. The peculiarity of a typical  $6 \mu\text{m} \times 3 \mu\text{m}$  a-CTP structure is shown in Figure 1c, where two normalized PL spectra are presented taken at an estimated absorbed pump power  $P \sim 100 \mu\text{W}$ . In the case of Figure 1c, the TP emission is only weakly detuned with respect to QW emission. The two spectra correspond to the emission from the two split fundamental CTP modes which are orthogonally polarized along X and Y, namely, parallel to the short and long side of the rectangle, respectively. The measured X- and Y-polarized spectra are characterized by the same spectral shape, and, most importantly, they feature a wavelength splitting of about 0.3 nm. The shorter wavelength peak corresponds to the X-polarized mode, while the longer wavelength one to the Y-polarized mode.

**Polarized Laser Emission.** Polarization-resolved PL experiments, by increasing the optical pump power  $P$  (pump

wavelength 780 nm), have been carried out to demonstrate a polarized lasing effect from the fundamental mode of a-CTPs and are summarized in Figure 2. These experiments were performed on a  $7 \mu\text{m} \times 3.5 \mu\text{m}$  microrectangle. Indeed, although this structure presents a slightly lower fundamental mode splitting than a  $6 \mu\text{m} \times 3 \mu\text{m}$  rectangle ( $\sim 0.2 \text{ nm}$ , see Figure 2b), its quality factor is slightly better, as it is discussed in Numerical Calculations. The integrated peaks intensities of the two orthogonal TE linear polarizations (parallel to the two sides of the rectangle) are shown in Figure 2(a) as a function of  $P$  in log–log scale. The Y-polarized integrated PL emission clearly shows a threshold behavior: when the excitation power is increased above  $P \sim 150 \mu\text{W}$ , a strong superlinear increase of PL integrated intensity from the longer wavelength zero-order CTP mode sets up, indicating the presence of a lasing effect. On the contrary, the X-polarized integrated emission does keep the same slope: no evidence of lasing behavior has been observed in the available range of pump powers, and the PL integrated intensity remains about 1 order of magnitude lower at the maximum excitation power.

PL spectra obtained by integration over all the far-field emission angles, and corresponding to two orthogonal angles of linear polarization ( $90^\circ$  for X,  $0^\circ$  for Y), are reported in Figure 2b,c, for a pump power value well below ( $P \sim 104 \mu\text{W}$ ) and well above ( $P \sim 187 \mu\text{W}$ ) threshold, respectively. For each of the two excitation powers, the normalized integrated PL intensity as a function of the angle of the analyzed linear polarization is also shown in a separate polar plot. At low pump power (Figure 2b),  $P \sim 104 \mu\text{W}$ , the recorded spectra have comparable intensities and similar spectral shape, proving that the two weakly split modes ( $\sim 0.2 \text{ nm}$ ) experience the same regime of light emission. The associated polar plot clearly shows that the normalized integrated PL has comparable intensity for every measured angle of linear polarization in between  $0^\circ$  and  $360^\circ$ , meaning that the TE polarization is randomly oriented in the plane of the structure. At high pump power (Figure 2c),  $P \sim 187 \mu\text{W}$ , the collected spectra are dramatically different, demonstrating that, even if the splitting is weak, the two modes experience strongly unequal interaction with the gain medium. The Y-polarized fundamental mode intensity is about 10 times higher than the X-polarized one, and the line width of the former is significantly narrower, implying an increased temporal coherence due to the onset of lasing action, completely absent in the case of the orthogonal polarization. In addition, the polar plot associated with this excitation power features a clear anisotropy of the PL intensity angular distribution, corresponding to a degree of linear polarization  $\text{DOP} = (I_{\text{max}} - I_{\text{min}})/(I_{\text{max}} + I_{\text{min}}) \approx 91.2\%$ , confirming that the emitted light is highly Y-polarized.

The selection of a linearly polarized laser emission is achieved by suppressing lasing action in the orthogonal polarization state, thus, maintaining a given polarization at the output with a high rejection ratio. In order to explain the physical mechanism responsible for linearly polarized laser emission, we have measured laser curves for different spectral detuning between the QW gain and the Tamm mode for a  $7 \mu\text{m} \times 3.5 \mu\text{m}$  rectangular metallic pattern. The detuning can be experimentally controlled thanks to the growth thickness gradient along the wafer, enabling a precise spectral tuning of the CTPs by changing the working position on the sample. The results are summarized in Figure 3a, where the absorbed pump power at the lasing threshold is plotted as a function of the spectral detuning  $\Delta$  between the QWs gain and the Tamm mode.

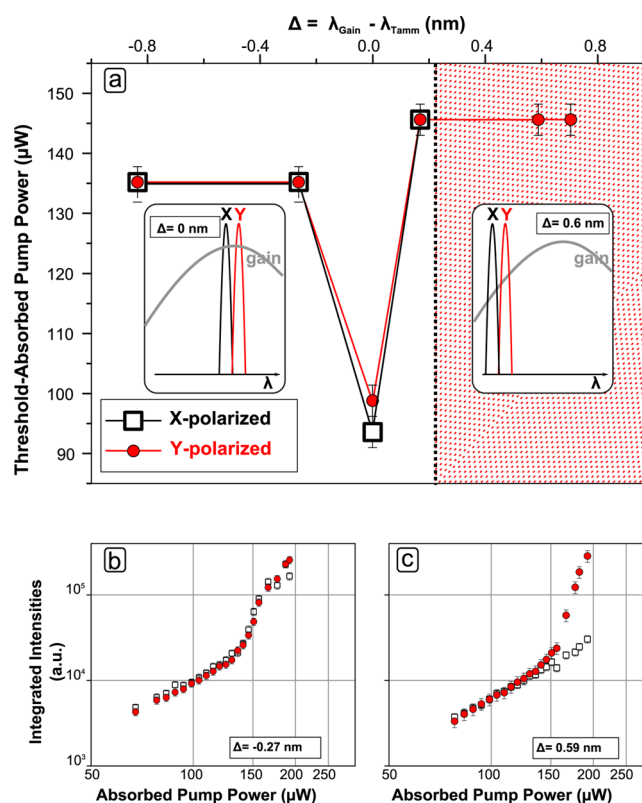


**Figure 3.** Lasing measurements on  $7 \mu\text{m} \times 3.5 \mu\text{m}$  a-CTP devices at different energy detuning. (a) Estimated absorbed pump power at threshold as a function of Gain-Tamm ( $\Delta$ ) wavelength detuning for X- and Y-polarized emission: only for  $\Delta = 0.59 \text{ nm}$  and  $0.7 \text{ nm}$  a single Y-polarized lasing threshold has been reported. Two detuning configurations are schematically shown in the insets. (b, c) Threshold curves taken at  $\Delta = -0.27 \text{ nm}$  and  $0.59 \text{ nm}$ , respectively, exhibiting the two different lasing behaviors.

Although the spectral position of the gain does not appear directly in experiments,<sup>44</sup> it is possible to extract the detuning between the QW exciton and the Tamm mode from low power experiments (see Supporting Information). The gain maximum is shifted from the excitonic transition but a quantitative evaluation of this energy shift in QW lasers is difficult to make, a priori.<sup>45</sup> However, we can affect the detuning value  $\Delta = 0 \text{ nm}$  to the minimum of the threshold curve (see Figure 3a), as it clearly comes from a maximum overlap between the QWs gain and the fundamental Tamm states.

Two main lasing behaviors can be observed within the spanned detuning range. For large positive detuning ( $\Delta > 0.2 \text{ nm}$ , hatched region in Figure 3a) the lasing action occurs only for the Y-polarized fundamental mode. We were not able to reach the threshold for the X polarization. This difference in threshold between the two directions of polarization appears in the input-output curve of Figure 3c ( $\Delta = 0.59 \text{ nm}$ ), where we can observe a behavior similar to that reported in Figure 2a. For detunings  $\Delta < 0.2 \text{ nm}$ , we observe that both orthogonal polarizations have roughly the same lasing threshold. A typical input-output curve is given in Figure 3b ( $\Delta = -0.27 \text{ nm}$ ). Consequently, for these devices, the resulting laser emission is unpolarized. In this spectral region, changing the detuning only affects the value of the threshold, with an optimum for zero detuning as discussed above, and an increase by a factor of 1.4 for the other devices. This threshold increase is a direct consequence of the strong dependence of the gain curve with respect to the wavelength.

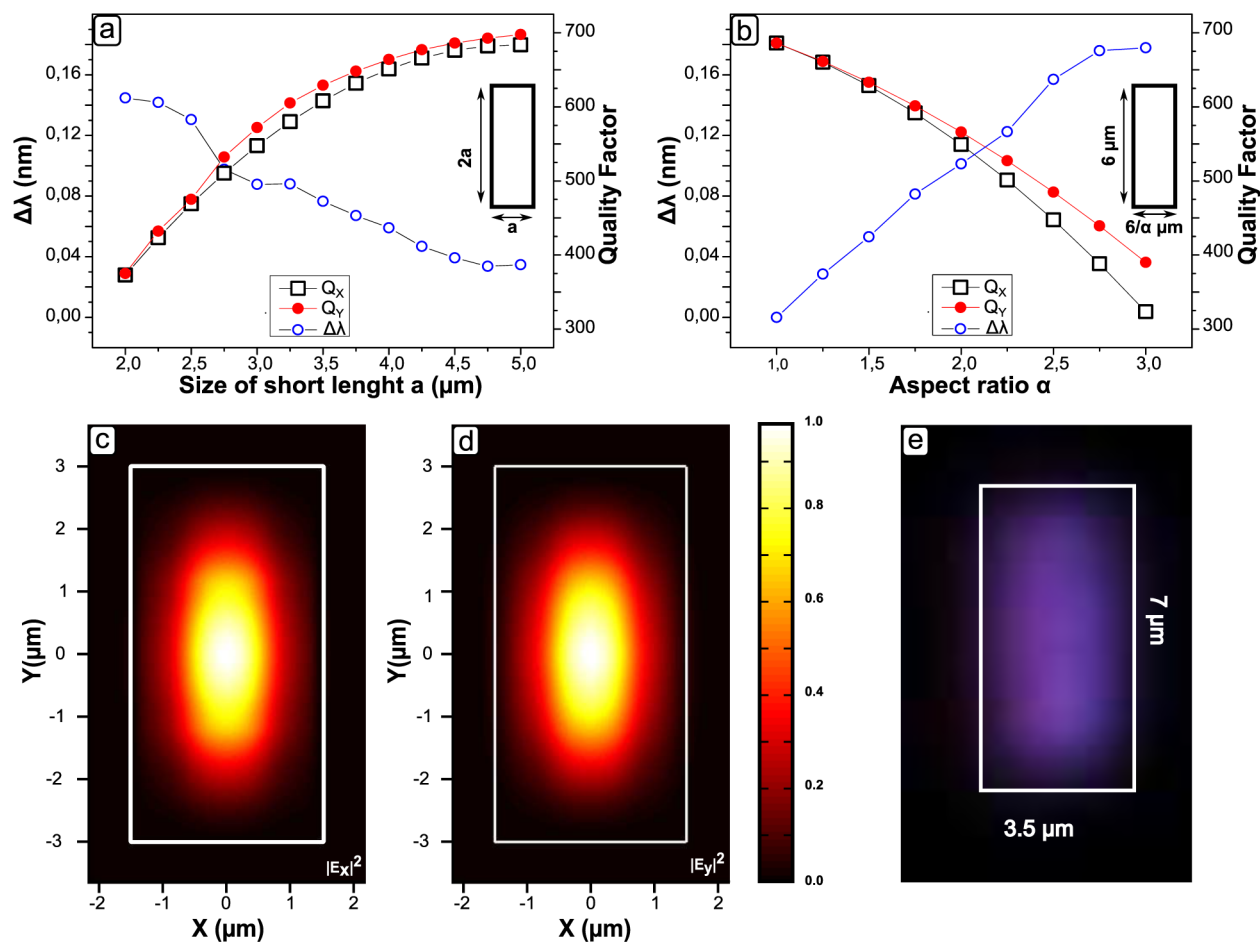


**Figure 4.** Numerical results from aperiodic Fourier modal method calculations. Wavelength splittings  $\Delta\lambda = \lambda_y - \lambda_x$  (empty blue circle) and quality factors of the  $Y$ - and  $X$ -polarized fundamental Tamm mode (red circle and empty black square, respectively) calculated (a) for different lateral sizes with a fixed aspect ratio of 2; and (b) for a rectangular geometry with aspect ratio ranging between 1 and 3 (long side size fixed at  $6 \mu\text{m}$ ). Fundamental modes normalized intensity distributions in the plane of a  $6 \mu\text{m} \times 3 \mu\text{m}$  rectangle for (c)  $E_x$  and (d)  $E_y$ . (e) Real space image of the top of a  $7 \mu\text{m} \times 3.5 \mu\text{m}$  lasing a-CTP device.

There are two physical parameters, induced by the anisotropic confinement, that can explain the polarized laser emission, namely the energy splitting between the two modes and their difference in quality factor. The polarization-induced splittings between these values are very weak: for the  $7 \mu\text{m} \times 3.5 \mu\text{m}$  structure under study, the  $Y$ -polarized fundamental mode lies  $\sim 0.2 \text{ nm}$  above the  $X$ -polarized mode, and its quality factor is only  $\sim 3\%$  better (see Numerical Calculations, Figure 4a). A qualitative explanation for the polarization selection when  $\Delta > 0.2 \text{ nm}$  is that, in this detuning range, the mode overlap with the gain curve is better for the  $Y$ -polarized mode than for the  $X$ -polarized mode. A very schematic layout of this process is given in the inset in Figure 3a, for a positive and zero detuning. Hence, when gain-clamping mechanism takes over, only the CTP fundamental mode polarized along  $Y$  direction can overcome losses. It should be noted that this polarization selection occurs only for positive detunings. The absence of  $X$ -polarization for negative detuning can be explained by the higher order Tamm confined modes lying at lower wavelength (see Figure 1b), generating complex multi-mode emission. The polarization selection is thus obtained by the interplay of two effects. On one hand, we have the anisotropy of the bidimensional metal geometry confining the TP mode. This is crucial for clearly removing the inherent polarization degeneracy, and it is responsible for introducing a

weak energy splitting between the two orthogonal polarization states. On the other hand, we have the spectral misalignment between the CTPs and the QWs gain. This allows for reducing the gain overlap with one of the two weakly split eigenmodes, as to make lasing condition possible only for the orthogonal one.

**Numerical Calculations.** Theoretical studies have also been carried out in order to support experimental observations as well as to provide some general trends for the design of polarized Tamm lasers. The anisotropic confined Tamm modes have been numerically calculated with the aperiodic Fourier modal method (a-FMM).<sup>46</sup> The modes, which are poles of the scattering matrix, are calculated with an iterative solving of Maxwell's equations in the complex frequency plane.<sup>47</sup> The refractive indices  $n$  used in the calculations are  $n_{\text{GaAs}} = 3.6633$ ,  $n_{\text{AlAs}} = 3.0179$ , and  $n_{\text{AlGaAs}} = 3.5345$ . For the permittivity of silver, we have used a Drude model that fits the data tabulated by Johnson and Christy around  $\lambda = 850 \text{ nm}$ .<sup>48</sup> As it has been shown in the previous section, the crucial parameter for a polarized lasing is the energy splitting between the two polarized modes. Figure 4a shows the calculated mode splitting and the quality factors when varying the length of the short side ( $X$  direction) of the rectangle, keeping a constant aspect ratio of 2. Largest rectangles feature a very small mode splitting (around  $0.04 \text{ nm}$ ), which increases above  $0.1 \text{ nm}$  when reducing the short size of the rectangle.

On the opposite, quality factors calculated for the  $X$ - and  $Y$ -polarized modes decrease strongly when decreasing the size of the structure. These additional losses with the size reduction have already been observed for isotropic Tamm modes.<sup>24,39</sup> For the  $6\ \mu\text{m} \times 3\ \mu\text{m}$  rectangle, a wavelength splitting of  $\sim 0.1\ \text{nm}$  is obtained from calculations, with the  $X$ -polarized mode sitting at shorter wavelength and the  $Y$ -polarized one at longer wavelength. This numerical result turns out to be in qualitative agreement with the experimental results presented in Figure 1c. The calculated quality factor of 550 ( $X$ -polarized mode) and 570 ( $Y$ -polarized mode) are also in qualitative agreement with the experimental value of 790 (see Supporting Informations). In Figure 4b, we present the calculated mode splitting and quality factors as a function of the aspect ratio, with a long side of the rectangle ( $Y$  direction) fixed at  $6\ \mu\text{m}$ . It also appears that the mode splitting increases with the aspect ratio (even if it tends to saturate), and that the quality factors for both polarizations decrease when the short side length is reduced. The optimization of the splitting has to be done keeping the quality factor relatively high to allow lasing in the structure.<sup>39</sup> A good trade-off is thus to use rectangles with a short side between 3 and  $3.5\ \mu\text{m}$ , and an aspect ratio around 2. Figure 4c,d shows the calculated normalized intensity distribution in the  $XY$ -plane lying 4 nm beneath the metallic disk for the two components  $E_X$  and  $E_Y$  of the fundamental mode electric field. The spatial profiles of the two field intensities have a similar shape and are in qualitative agreement with the intensity distribution measured on a CCD camera for an a-CTP device under  $Y$ -polarized lasing operation (Figure 4e).

## CONCLUSIONS

We have demonstrated that Tamm plasmon modes can be confined in all space dimensions by means of 2D anisotropic metallic patterns on top of a DBR, and we call these structures a-CTPs. In particular, a-CTPs made of silver microrectangles having an aspect ratio of 2 ( $7\ \mu\text{m} \times 3.5\ \mu\text{m}$ ) have been observed to split the fundamental mode into two modes orthogonally polarized along the two sides of the rectangle. Though weak, such a splitting has been observed to lead to a linearly polarized laser emission featuring a degree of linear polarization in excess of 90%, given that the Tamm-gain energy detuning is properly controlled. Our achievements show that a-CTPs are very promising candidates as semiconductor-integrated surface-emitting laser sources operating at a stable single-mode linear polarization. These easily controllable polarized compact laser sources can be of large interest for applications in spectroscopy, polarization-dependent optical setups and low-noise high-speed data transmission over single-mode optical fibers. Besides the easy and versatile patterning of the metallic film, the semiconductor part of the structure is not affected by any etching process. Thus, the electrical and technological schemes already developed for electrical excitation could be implemented for Tamm lasers as well.

## ASSOCIATED CONTENT

### Supporting Information

Experimental procedure for the extraction of the detuning between the Tamm mode and the exciton, as well as for the quality factor. The Supporting Information is available free of charge on the ACS Publications website at DOI: 10.1021/ph500467s.

## AUTHOR INFORMATION

### Corresponding Author

\*E-mail: clementine.symonds@univ-lyon1.fr.

## Notes

The authors declare no competing financial interest.

## ACKNOWLEDGMENTS

The authors acknowledge financial support from LabEx iMUST of Université de Lyon on research project “TaPaS”, and from Agence Nationale de la Recherche (ANR) on ANR Project “NEHMESIS”.

## REFERENCES

- (1) Yariv, A.; Ye, P. *Photonics: Optical Electronics in Modern Communications*; Oxford University Press: New York, 2009.
- (2) Nielsen, M.; Chuang, I. *Quantum Computation and Quantum Information*; Cambridge University Press: New York, 2000.
- (3) De La Rue, R.; Lourtioz, J.-M.; Yu, S. *Compact Semiconductor Lasers*; Wiley: New York, 2014.
- (4) Matsuda, N.; le Jeannic, H.; Fukuda, H.; Tsuchizawa, T.; Munro, W. J.; Shimizu, K.; Yamada, K.; Tokura, Y.; Takesue, H. A monolithically integrated polarization entangled photon pair source on a silicon chip. *Sci. Rep.* **2012**, *2*, 817.
- (5) Crespi, A.; Ramponi, R.; Osellame, R.; Sansoni, L.; Bongioanni, I.; Sciarino, F.; Vallone, G.; Mataloni, P. Integrated photonic quantum gates for polarization qubits. *Nat. Commun.* **2011**, *2*, 566.
- (6) Coldren, L.; Corzine, S.; Mashanovitch, M. *Diode Lasers and Photonic Integrated Circuits*; Wiley: New York, 2012.
- (7) Chow, W.; Choquette, K.; Crawford, M.; Lear, K.; Hadley, G. Design, fabrication, and performance of infrared and visible vertical-cavity surface-emitting lasers. *IEEE J. Quantum Electron.* **1997**, *33*, 1810–1824.
- (8) Verschuren, M.; Gerlach, P.; van Sprang, H.; Polman, A. Improved performance of polarization-stable VCSELs by monolithic sub-wavelength gratings produced by soft nano-imprint lithography. *Nanotechnology* **2011**, *22*, 505201.
- (9) Gauthier, J.-P.; Paranthoën, C.; Levallois, C.; Shuaib, A.; Lamy, J.; Folliot, H.; Perrin, M.; Dehaese, O.; Chevalier, N.; Durand, O.; Le Corre, A. Enhancement of the polarization stability of a  $1.55\ \mu\text{m}$  emitting vertical-cavity surface-emitting laser under modulation using quantum dashes. *Opt. Express* **2012**, *20*, 16832–16837.
- (10) Tan, M. P.; Member, S.; Kasten, A. M.; Strand, T. A.; Choquette, K. D. Polarization switching in vertical-cavity surface-emitting lasers with anisotropic cavity geometry and injection. *IEEE Photonics Technol. Lett.* **2012**, *24*, 745–747.
- (11) Tan, M. P.; Kasten, A. M.; Sulkin, J. D.; Choquette, K. D. Planar photonic crystal vertical-cavity surface-emitting lasers. *IEEE J. Sel. Top. Quantum Electron.* **2013**, *19*, 4900107–4900107.
- (12) Pan, Z. G.; Jiang, S.; Dagenais, M.; Morgan, R. A.; Kojima, K.; Asom, M. T.; Leibenguth, R. E.; Guth, G. D.; Focht, M. W. Optical injection induced polarization bistability in vertical cavity surface-emitting lasers. *Appl. Phys. Lett.* **1993**, *63*, 2999–3001.
- (13) Choquette, K.; Richie, D.; Leibenguth, R. Temperature dependence of gain-guided vertical-cavity surface emitting laser polarization. *Appl. Phys. Lett.* **1994**, *64*, 2062.
- (14) Choquette, K. D.; Schneider, R. P.; Kevin, L. L.; Leibenguth, R. E. Gain-dependent polarization properties of vertical-cavity lasers. *IEEE J. Sel. Top. Quantum Electron.* **1995**, *1*, 661–666.
- (15) Uenohara, H.; Tateno, K.; Kagawa, T.; Ohiso, Y.; Tsuda, H.; Kurokawa, T.; Amano, C. Investigation of dynamic polarization stability of 850 nm GaAs-based vertical-cavity surface-emitting lasers grown on (311)B and (100) substrates. *IEEE Photonics Technol. Lett.* **1999**, *11*, 400.
- (16) Niskiyama, N.; Arai, M.; Shinada, S.; Azuchi, M.; Miyamoto, T.; Koyama, F.; Iga, K. Highly strained GaInAs-GaAs quantum-well vertical-cavity surface-emitting laser on GaAs (311)B substrate for stable polarization operation. *IEEE J. Sel. Top. Quantum Electron.* **2001**, *7*, 242.
- (17) Mukaiharu, T.; Koyama, F.; Iga, K. Engineering polarization control of GaAs/AlGaAs surface-emitting lasers by anisotropic stress

from elliptical etched substrate hole. *IEEE Photonics Technol. Lett.* **1993**, *5*, 133.

(18) Choquette, K.; Leibenguth, R. Control of vertical-cavity laser polarization with anisotropic transverse cavity geometries. *IEEE Photonics Technol. Lett.* **1994**, *6*, 40–42.

(19) Choquette, K. D.; Lear, K. L.; Leibenguth, R. E.; Asom, M. T. Polarization modulation of cruciform vertical-cavity laser diodes. *Appl. Phys. Lett.* **1994**, *64*, 2767–2769.

(20) Gayral, B.; Gerard, J. M.; Legrand, B.; Cuostard, E.; Thierry-Mieg, V. Optical study of GaAs/AlAs pillar microcavities with elliptical cross section. *Appl. Phys. Lett.* **1998**, *72*, 1421.

(21) Song, D.; Kim, S.; Park, H.; Kim, C.; Lee, Y. Single fundamental-mode photonic-crystal vertical-cavity surface-emitting lasers. *Appl. Phys. Lett.* **2002**, *80*, 3901.

(22) Danner, A.; Rafferty, J.; Yokouchi, N.; Choquette, K. Transverse modes of photonic crystal vertical-cavity lasers. *Appl. Phys. Lett.* **2004**, *84*, 1031.

(23) Yokouchi, N.; Danner, A.; Choquette, K. Two-dimensional photonic crystal confined vertical-cavity surface-emitting lasers. *IEEE J. Sel. Top. Quantum Electron.* **2003**, *9*, 1439.

(24) Gazzano, O.; de Vasconcellos, S. M.; Gauthron, K.; Symonds, C.; Bloch, J.; Voisin, P.; Bellessa, J.; Lemaître, A.; Senellart, P. Evidence for confined Tamm plasmon modes under metallic microdisks and application to the control of spontaneous optical emission. *Phys. Rev. Lett.* **2011**, *107*, 247402.

(25) Symonds, C.; Lemaître, A.; Senellart, P.; Jomaa, M.; Aberra Guebrou, S.; Homeyer, E.; Brucoli, G.; Bellessa, J. Lasing in a hybrid GaAs/silver Tamm structure. *Appl. Phys. Lett.* **2012**, *100*, 121122.

(26) Gazzano, O.; de Vasconcellos, S. M.; Gauthron, K.; Symonds, C.; Voisin, P.; Bellessa, J.; Lemaître, A.; Senellart, P. Single photon source using confined Tamm plasmon modes. *Appl. Phys. Lett.* **2012**, *100*, 23111.

(27) Kaliteevski, M.; Iorsh, I.; Brand, S.; Abram, R.; Chamberlain, J.; Kavokin, A.; Shelykh, I. Tamm plasmons-polaritons: Possible electromagnetic states at the interface of a metal and a dielectric Bragg mirror. *Phys. Rev. B* **2007**, *76*, 165415.

(28) Sasin, M. E.; Seisyan, R. P.; Kaliteevski, M. A.; Brand, S.; Abram, R. a.; Chamberlain, J. M.; Egorov, a. Y.; Vasil'ev, A. P.; Mikhlin, V. S.; Kavokin, a. V.; Kaliteevski, M. a.; Vasil'ev, a. P. Tamm plasmons-polaritons: Slow and spatially compact light. *Appl. Phys. Lett.* **2008**, *92*, 251112.

(29) Gong, Y.; Liu, X.; Lu, H.; Wang, L.; Wang, G. Perfect absorber supported by optical Tamm states in plasmonic waveguide. *Opt. Express* **2011**, *19*, 18393–18398.

(30) Zhou, H.; Yang, G.; Wang, K.; Long, H.; Lu, P. Multiple optical Tamm states at a metal-dielectric mirror interface. *Opt. Lett.* **2010**, *35*, 4112–4114.

(31) Zhang, W.; Yu, S. Bistable switching using an optical Tamm cavity with a Kerr medium. *Opt. Commun.* **2010**, *283*, 2622–2626.

(32) Lee, K. J.; Wu, J. W.; Kim, K. Enhanced nonlinear optical effects due to the excitation of optical Tamm plasmon polaritons in one-dimensional photonic crystal structures. *Opt. Express* **2013**, *21*, 28817–28823.

(33) Badugu, R.; Descrovi, E.; Lakowicz, J. R. Radiative decay engineering 7: Tamm state-coupled emission using a hybrid plasmonic-photonic structure. *Anal. Biochem.* **2014**, *445*, 1–13.

(34) Chen, Y.; Zhang, D.; Qiu, D.; Zhu, L.; Yu, S.; Yao, P.; Wang, P.; Ming, H.; Badugu, R.; Lakowicz, J. R. Back focal plane imaging of Tamm plasmons and their coupled emission. *Laser Photonics Rev.* **2014**, *8*, 933–940.

(35) Chen, Y.; Zhang, D.; Zhu, L.; Wang, R.; Wang, P.; Ming, H.; Badugu, R.; Lakowicz, J. R. Tamm plasmon- and surface plasmon-coupled emission from hybrid plasmonic-photonic structures. *Optica* **2014**, *1*, 407–413.

(36) Auguie, B.; Fuertes, M. C.; Angelomé, P. C.; Abdala, N. L.; Soler Illia, G. J. A. A.; Fainstein, A. Tamm plasmon resonance in mesoporous multilayers: Toward a sensing application. *ACS Photonics* **2014**, *1*, 775–780.

(37) Afinogenov, B.; Bessonov, V.; Nikulin, A.; Fedyanin, A. Observation of hybrid state of Tamm and surface plasmon-polaritons in one-dimensional photonic crystals. *Appl. Phys. Lett.* **2013**, *103*, 1–4.

(38) Lopez-Garcia, M.; Ho, Y.-L.; Taverne, M.; Chen, L.-F.; Murshidy, M.; Edwards, A.; Serry, M.; Adawi, A.; Rarity, J.; Oulton, R. Efficient out-coupling and beaming of Tamm optical states via surface plasmon polariton excitation. *Appl. Phys. Lett.* **2014**, *104*, 1–5.

(39) Symonds, C.; Lheureux, G.; Hugonin, J.-P.; Greffet, J.-J.; Laverdant, J.; Brucoli, G.; Lemaître, A.; Senellart, P.; Bellessa, J. Confined Tamm plasmon lasers. *Nano Lett.* **2013**, *13*, 3179–3184.

(40) Ramaswamy, V.; French, W. G.; Standley, R. D. Polarization characteristics of noncircular core single-mode fibers. *Appl. Opt.* **1978**, *17*, 3014–3017.

(41) Stanley, R. P.; Houdré, R.; Weisbuch, C.; Oesterle, U.; Ilegems, M. Cavity-polariton photoluminescence in semiconductor microcavities: Experimental evidence. *Phys. Rev. B* **1996**, *53*, 10995–11007.

(42) Reithmaier, J.; Röhner, M.; Zull, H.; Schäfer, F.; Forchel, A.; Knipp, P.; Reinecke, T. Size dependence of confined optical modes in photonic quantum dots. *Phys. Rev. Lett.* **1997**, *78*, 378–381.

(43) Symonds, C.; Lemaître, A.; Homeyer, E.; Plenet, J. C.; Bellessa, J. Emission of Tamm plasmon/exciton polaritons. *Appl. Phys. Lett.* **2009**, *95*, 200995.

(44) Hakki, B.; Paoli, T. Gain spectra in GaAs double-heterostructure injection lasers. *J. Appl. Phys.* **1975**, *46*, 1299.

(45) Schmitt-Rink, S.; Ell, C.; Haug, H. Many-body effects in the absorption, gain, and luminescence spectra of semiconductor quantum-well structures. *Phys. Rev. B* **1986**, *33*, 1183–1189.

(46) Silberstein, E.; Lalanne, P.; Hugonin, J.-P.; Cao, Q. Use of grating theories in integrated optics. *J. Opt. Soc. Am. A* **2001**, *18*, 2865–2875.

(47) Bai, Q.; Perrin, M.; Sauvan, C.; Hugonin, J.-P.; Lalanne, P. Use of grating theories in integrated optics. *Opt. Express* **2013**, *21*, 27371.

(48) Johnson, P.; Christy, R. Optical constants of noble metal. *Phys. Rev. B* **1972**, *6*, 4370–4379.